Accounting for the ultraviolet divergence in field-theoretic simulations of block copolymer melts

View Online   Export Citation   CrossMark

M. W. Matsen,[1,2,3,a)] **T. M. Beardsley,**[1,2,3] **and J. D. Willis**[2]

AFFILIATIONS

[1] Department of Chemical Engineering, University of Waterloo, Waterloo, Ontario N2L 3G1, Canada
[2] Department of Physics and Astronomy, University of Waterloo, Waterloo, Ontario N2L 3G1, Canada
[3] Waterloo Institute for Nanotechnology, University of Waterloo, Waterloo, Ontario N2L 3G1, Canada

[a)]Author to whom correspondence should be addressed: mwmatsen@uwaterloo.ca

ABSTRACT

This study examines the ultraviolet (UV) divergence in field-theoretic simulations (FTSs) of block copolymer melts, which causes an unphysical dependence on the grid resolution, Δ, used to represent the fields. Our FTSs use the discrete Gaussian–chain model and a partial saddle-point approximation to enforce incompressibility. Previous work has demonstrated that the UV divergence can be accounted for by defining an effective interaction parameter, $\chi = z_\infty \chi_b + c_2 \chi_b^2 + c_3 \chi_b^3 + \cdots$, in terms of the bare interaction parameter, χ_b, used in the FTSs, where the coefficients of the expansion are determined by a Morse calibration. However, the need to use different grid resolutions for different ordered phases generally restricts the calibration to the linear approximation, $\chi \approx z_\infty \chi_b$, and prevents the calculation of order–order transitions. Here, we resolve these two issues by showing how the nonlinear calibration can be translated between different grids and how the UV divergence can be removed from free energy calculations. By doing so, we confirm previous observations from particle-based simulations. In particular, we show that the free energy closely matches self-consistent field theory (SCFT) predictions, even in the region where fluctuations disorder the periodic morphologies, and similarly, the periods of the ordered phases match SCFT predictions, provided the SCFT is evaluated with the nonlinear χ.

*Published under an exclusive license by AIP Publishing.* https://doi.org/10.1063/5.0134890

I. INTRODUCTION

Block copolymers are a special class of polymers, where the chain is divided into chemically distinct blocks.[1] The simplest is the AB diblock architecture, where the chain consists of a block of N_A A-type segments, joined to a block of N_B B-type segments. Due to the general immiscibility of dissimilar components, a melt of diblock copolymers will tend to segregate into A- and B-rich domains. However, the domains remain microscopic in size, due to the connectivity of the blocks, resulting in the formation of periodically ordered microstructures. Figure 1 shows a theoretical phase diagram for diblock copolymer melts. The ordered microstructures form once $\chi N \gtrsim 10$, where $N = N_A + N_B$ and χ is the Flory–Huggins parameter, measuring the incompatibility of the A and B components. The geometry of the microstructure is generally controlled by

the composition of the diblock, $f = N_A/N$. The stable microstructures include the classical lamellar, cylindrical, and spherical phases, as well as two network phases, referred to as gyroid[4,5] and Fddd.[6,7]

The phase behavior of block copolymer melts is understood to be universal,[8–11] meaning that all chemically distinct molecules and theoretical models become equivalent at large N. As such, they can all be mapped onto the standard Gaussian–chain model (GCM),[12] which treats the system as an incompressible melt of continuous elastic threads, interacting with pairwise contact forces. In the case of a diblock copolymer melt, the polymer paths are denoted by space curves, $\mathbf{r}_\alpha(t)$, where $\alpha \in \{1, 2, \ldots, n\}$ labels the polymers, and $t \in [0, N]$ indexes the segments along the polymer contours. The Hamiltonian for the GCM,

$$H_p[\{\mathbf{r}_\alpha\}] = U_b[\{\mathbf{r}_\alpha\}] + U_{\text{int}}[\{\mathbf{r}_\alpha\}], \tag{1}$$
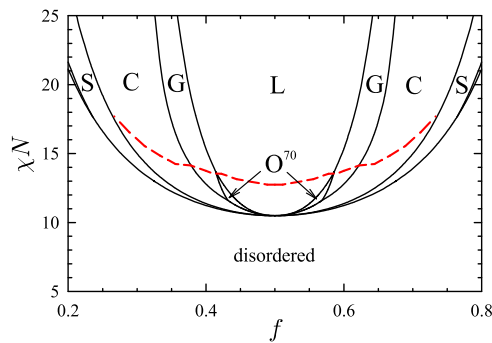
FIG. 1. Phase diagram for diblock copolymer melts, calculated using SCFT.[2] The ordered phases are lamellar (L), Fddd (O^{70}), gyroid (G), cylindrical (C), and spherical (S). The dashed curve shows the fluctuation-corrected ODT for $\bar{N} = 10^4$, calculated using FTSs.[3]

can be split into bonded interactions,

$$\frac{U_b}{k_B T} = \frac{3}{2a^2} \sum_{\alpha=1}^{n} \int_0^N |\mathbf{r}'_\alpha(t)|^2 dt, \quad (2)$$

where a is the statistical length of a segment, and nonbonded interactions,

$$\frac{U_{\text{int}}}{k_B T} = \chi_b \rho_0 \int \hat{\phi}_A(\mathbf{r}) \hat{\phi}_B(\mathbf{r}) d\mathbf{r}, \quad (3)$$

where χ_b is the bare interaction strength and

$$\hat{\phi}_A(\mathbf{r}) = \frac{1}{\rho_0} \sum_{\alpha=1}^{n} \int_0^{N_A} \delta(\mathbf{r} - \mathbf{r}_\alpha(t)) dt, \quad (4)$$

$$\hat{\phi}_B(\mathbf{r}) = \frac{1}{\rho_0} \sum_{\alpha=1}^{n} \int_{N_A}^{N} \delta(\mathbf{r} - \mathbf{r}_\alpha(t)) dt \quad (5)$$

are dimensionless concentrations of the A and B segments, respectively. A uniform segment density of ρ_0 is enforced by constraining the polymer coordinates so that $\hat{\phi}_A(\mathbf{r}) + \hat{\phi}_B(\mathbf{r}) = 1$.

In polymer field theory,[13–15] the particle-based GCM is transformed to a mathematically equivalent field-based model, involving a composition field, $W_-(\mathbf{r})$, that couples to the difference in concentrations, $\hat{\phi}_-(\mathbf{r}) \equiv \hat{\phi}_A(\mathbf{r}) - \hat{\phi}_B(\mathbf{r})$, and a pressure field, $W_+(\mathbf{r})$, that couples to the total concentration, $\hat{\phi}_+(\mathbf{r}) \equiv \hat{\phi}_A(\mathbf{r}) + \hat{\phi}_B(\mathbf{r})$, in a system of noninteracting polymers. The field-based Hamiltonian, $\tilde{H}_f[W_-, W_+]$, takes the form

$$\frac{\tilde{H}_f}{n k_B T} = -\ln Q + \frac{\chi_b N}{4} + \frac{\rho_0}{n} \int \left(\frac{W_-^2(\mathbf{r})}{\chi_b} - W_+(\mathbf{r}) \right) d\mathbf{r}, \quad (6)$$

where $Q[W_-, W_+]$ is the partition function for a single molecule in the system of noninteracting polymers.

The mean-field approximation of the model is known as self-consistent field theory (SCFT).[16] It approximates the free energy by $F = \tilde{H}_f[w_-, w_+]$, where $w_-(\mathbf{r})$ and $w_+(\mathbf{r})$ denote the saddle point

of the Hamiltonian. The saddle point is obtained by solving the self-consistent conditions

$$\phi_-(\mathbf{r}) = -\frac{2}{\chi_b} W_-(\mathbf{r}), \quad (7)$$

$$\phi_+(\mathbf{r}) = 1, \quad (8)$$

where $\phi_\pm(\mathbf{r})$ are ensemble averages of $\hat{\phi}_\pm(\mathbf{r})$ in the system of noninteracting polymers. In general, there are multiple solutions corresponding to different metastable phases; the one of lowest free energy represents the stable phase. The phase diagram in Fig. 1 was calculated using SCFT.[2]

SCFT is understood to be exact in the limit of infinite molecular weight,[17] but there are significant perturbations to the phase diagram at finite molecular weights. For instance, they push the order-disorder transition (ODT) to higher χN, creating direct transitions between the different ordered phases and the disordered phase. The size of the fluctuation corrections is controlled by the invariant polymerization index[18]

$$\bar{N} = a^6 \rho_0^2 N, \quad (9)$$

which typically ranges between 10^2 and 10^4 in experimental systems.[19,20] Field-theoretic simulations (FTSs) provide a means of evaluating fluctuation corrections by simulating the Hamiltonian $\tilde{H}_f[W_-, W_+]$.[15,21] One complication, however, is that the pressure field, $W_+(\mathbf{r})$, enforcing incompressibility is imaginary, which leads to a complex-valued Hamiltonian and, thus, a Boltzmann weight that is not positive definite. Fredrickson and coworkers have dealt with this problem by performing complex Langevin simulations (CL-FTSs).[21–25] An alternative strategy is to perform a partial saddle-point approximation,[26–28] where the composition field, $W_-(\mathbf{r})$, fluctuates, while the pressure field follows its saddle point, $w_+(\mathbf{r})$. The saddle point turns out to be real and, consequently, so is the Hamiltonian $\tilde{H}_f[W_-, w_+]$, which thereby allows for standard simulation techniques. The ODT for $\bar{N} = 10^4$ in Fig. 1 was obtained using this variant of FTSs.[3]

In FTSs, the fields are represented on a discrete grid with finite spacings, Δ_ν, in the $\nu = x$, y, and z directions. One might expect results to become increasingly accurate as $\Delta_\nu \to 0$, but this is not the case for the standard GCM, due to an ultraviolet (UV) divergence.[29–31] Although the model defines the interactions as contact forces, in practice, the range is dictated by the grid spacing. Consequently, the number of intermolecular interactions is reduced as the grid resolution becomes finer, which lowers the segregation. Beardsley and Matsen[32] addressed this by expressing results in terms of an effective interaction parameter

$$\chi = z_\infty \chi_b + c_2 \chi_b^2 + c_3 \chi_b^3 + \cdots, \quad (10)$$

where the coefficients are determined by the Morse calibration,[9,33,34] originally devised for particle-based simulations. The first coefficient, z_∞, is the relative number of intermolecular contacts in the limit of $\chi_b \to 0$ and $N \to \infty$. For continuous chains,

$$z_\infty = 1 - \frac{1}{V_{\text{cell}} \rho_0} \int_{-\infty}^{\infty} P(t), \quad (11)$$

where V_{cell} is the volume associated with each grid point and

$$P(t) = \prod_v \frac{\Delta_v}{a} \sqrt{\frac{3}{2\pi|t|}} \, \text{erf}\left(\frac{\pi a}{\Delta_v}\sqrt{\frac{|t|}{6}}\right) \quad (12)$$

is the probability that two segments of a polymer, separated by a distance t along the chain contour, occupy the same grid point. The remaining coefficients are determined by fitting the peak of the disordered-state structure function, $S(k)$, for symmetric diblock copolymers to renormalized one-loop (ROL) predictions.[35,36] Note, Ref. 32 has shown that the linear approximation, $\chi \approx z_\infty \chi_b$, is equivalent to an earlier renormalization by Stasiak and Matsen.[30]

The fluctuation-corrected ODT in Fig. 1 was plotted using the linear χ, rather than the more accurate nonlinear χ. This is because the periods of the ordered phases differ along the ODT, which necessitates the use of different grids. As a result, the coefficients of the Morse calibration would have to be re-evaluated at each point along the transition. The need for distinct grids also inhibits the calculation of order–order transitions (OOTs). The aim of this paper is to resolve these two issues.

II. THEORY AND SIMULATION

Our FTSs are performed in $L_x \times L_y \times L_z$ orthorhombic simulation boxes with periodic boundary conditions. Note that the dimensions of the box will generally be expressed in terms of $R_0 = aN^{1/2}$. The boxes are overlaid with $m_x \times m_y \times m_z$ grids of uniform spacing, $\Delta_v = L_v/m_v$, in the $v = x$, y, and z directions. Hence, the total volume of a box is $V = L_x L_y L_z$, and the total number of grid points is $M = m_x m_y m_z$. The Hamiltonian, $\tilde{H}[W_-, w_+]$, is then simulated using conventional Langevin dynamics.[37]

Here, we modify the standard GCM by switching from continuous to discrete chains,[38] each consisting of N beads, connected by harmonic springs. The polymer coordinates of the discrete model are specified by the set of vectors $\{\mathbf{r}_{\alpha,i}\}$, where $i \in \{1, 2, \ldots, N\}$ is the monomer index. With this modification, the energy of the bonded interactions becomes

$$\frac{U_b}{k_B T} = \frac{3}{2a^2} \sum_{\alpha=1}^n \sum_{i=1}^{N-1} |\mathbf{r}_{\alpha,i+1} - \mathbf{r}_{\alpha,i}|^2, \quad (13)$$

and the dimensionless A and B concentrations become

$$\hat{\phi}_A(\mathbf{r}) = \frac{1}{\rho_0} \sum_{\alpha=1}^n \sum_{i=1}^{N_A} \delta(\mathbf{r} - \mathbf{r}_{\alpha,i}), \quad (14)$$

$$\hat{\phi}_B(\mathbf{r}) = \frac{1}{\rho_0} \sum_{\alpha=1}^n \sum_{i=N_A+1}^{N} \delta(\mathbf{r} - \mathbf{r}_{\alpha,i}), \quad (15)$$

respectively. A detailed algorithm and sample source code are provided in Ref. 28.

The switch from continuous to discrete chains avoids numerical inaccuracies in solving the theory,[39,40] and also leads to a more natural implementation of the Morse calibration. There is no cost of doing so,[32] since the Morse calibration used to remove the UV divergence simultaneously accounts for the modification to the model. In that regard, the first coefficient of the Morse calibration changes to

$$z_\infty = 1 - \frac{1}{V_{\text{cell}}\rho_0} \sum_{i=-\infty}^{\infty} P(i), \quad (16)$$

but the remaining coefficients, c_p for $p = 2, 3, \ldots$, are still determined by fitting the peak of $S(k)$ for symmetric diblocks to ROL theory.

A. UV divergence

In an effort to understand the UV divergence, we begin by considering homopolymer melts (i.e., $\chi_b \to 0$), where the free energy is generally set to zero. In this limit, the Hamiltonian reduces to

$$\frac{\tilde{H}_f}{k_B T} \approx \frac{\rho_0}{\chi_b} \int W_-^2(\mathbf{r}) d\mathbf{r} = \frac{\rho_0 V}{\chi_b M} \sum_{\mathbf{r}} W_-^2(\mathbf{r}), \quad (17)$$

which corresponds to a system of M harmonic oscillators with *spring constants* of $\kappa = 2\rho_0 V/\chi_b M$. It thus follows that the composition field at each grid point has an average value and variance of

$$\langle W_-(\mathbf{r}) \rangle = 0 \quad \text{and} \quad \langle W_-^2(\mathbf{r}) \rangle = \kappa^{-1}, \quad (18)$$

respectively. Although the field vanishes in the limit of $\chi_b \to 0$, the free energy of the M harmonic oscillators,

$$\frac{F_{\text{UV}}}{k_B T} = -\frac{M}{2} \ln\left(\frac{\chi_b M}{2\rho_0 V}\right), \quad (19)$$

nevertheless remains finite. This is the first consequence of the UV divergence, which will need to be removed from the total free energy.

The remaining effect of the UV divergence appears once χ_b becomes finite. To illustrate this, we now consider small χ_b, where the weak fields allow the single-chain partition function to be approximated by[14]

$$\ln \mathcal{Q} \approx -\frac{N}{V}[W_+(\mathbf{0}) + (2f-1)W_-(\mathbf{0})]$$
$$+ \frac{N^2}{2V^2} \sum_{s,t=\pm} \sum_{\mathbf{k}\neq 0} S_{st}(k) W_s(\mathbf{k}) W_t(-\mathbf{k}), \quad (20)$$

in terms of the Fourier transforms

$$W_\pm(\mathbf{k}) = \int W_\pm(\mathbf{r}) e^{i\mathbf{k}\cdot\mathbf{r}} d\mathbf{r}. \quad (21)$$

The coefficients of the expansion are given by

$$S_{--}(k) = \frac{1}{N^2} \sum_{i=1}^N \sum_{j=1}^N \gamma_i \gamma_j \exp(-x|i-j|), \quad (22)$$

$$S_{++}(k) = \frac{1}{N^2} \sum_{i=1}^N \sum_{j=1}^N \exp(-x|i-j|), \quad (23)$$

$$S_{+-}(k) = \frac{1}{N^2} \sum_{i=1}^N \sum_{j=1}^N \gamma_j \exp(-x|i-j|), \quad (24)$$

where $x \equiv k^2 a^2 / 6$, $\gamma_i = +1$ for $i \leq N_A$, and $\gamma_i = -1$ for $i > N_A$. By symmetry, $S_{-+}(k) = S_{+-}(k)$. The Fourier transforms of the composition, $\phi_-(\mathbf{k})$, and total concentration, $\phi_+(\mathbf{k})$, in the system of noninteracting polymers are given by

$$\phi_s(\mathbf{k}) = -\sum_{t=\pm} S_{st}(k) W_t(\mathbf{k}). \qquad (25)$$

Thus, the partial saddle-point approximation [i.e., $\phi_+(\mathbf{k}) = 0$ for $\mathbf{k} \neq 0$] requires

$$W_+(\mathbf{k}) = -\frac{S_{+-}(k)}{S_{++}(k)} W_-(\mathbf{k}). \qquad (26)$$

Substituting this into Eq. (20), we obtain

$$\ln \mathcal{Q} \approx -\frac{N}{V} \left[W_+(\mathbf{0}) + (2f - 1) W_-(\mathbf{0}) \right] + \frac{2N^2}{V^2} \sum_{\mathbf{k} \neq 0} \frac{W_-(\mathbf{k}) W_-(-\mathbf{k})}{\mathcal{F}(k)}, \qquad (27)$$

where

$$\mathcal{F}(k) = \frac{4 S_{++}(k)}{S_{++}(k) S_{--}(k) - S_{+-}^2(k)}. \qquad (28)$$

Substituting this into Eq. (6) gives

$$\frac{\tilde{H}_f}{k_B T} \approx \frac{\rho_0}{V \chi_b} \left\{ \left[W_-(\mathbf{0}) + V \chi_b \left(f - \frac{1}{2} \right) \right]^2 + \sum_{\mathbf{k} \neq 0} \left(1 - \frac{2 \chi_b N}{\mathcal{F}(k)} \right) W_-(\mathbf{k}) W_-(-\mathbf{k}) \right\} + n \chi_b N f(1 - f), \qquad (29)$$

which is again a Hamiltonian for M harmonic oscillators, but with slightly reduced spring constants relative to those of the homopolymer melt. As such, the free energy of the diblock copolymer melt is given by

$$\frac{\tilde{F}}{k_B T} = \frac{F_{\mathrm{UV}}}{k_B T} + \frac{1}{2} \sum_{\mathbf{k}} \ln \left(1 - \frac{2 \chi_b N}{\mathcal{F}(k)} \right) + n \chi_b N f(1 - f). \qquad (30)$$

Note that $\mathcal{F}(k)$ diverges for $k \to 0$, which justifies our inclusion of the $\mathbf{k} = 0$ term in the sum. Given that χ_b is small, the logarithm can be expanded to give

$$\frac{\tilde{F} - F_{\mathrm{UV}}}{n k_B T} = z_N \chi_b N f(1 - f), \qquad (31)$$

where

$$z_N = 1 - \frac{\sum_{\mathbf{k}} [\mathcal{F}(k)]^{-1}}{n f(1 - f)}. \qquad (32)$$

In the thermodynamic limit (i.e., $V \to \infty$), the sum becomes an integral and, therefore,

$$z_N = 1 - \frac{N \int [\mathcal{F}(k)]^{-1} d\mathbf{k}}{(2\pi)^3 \rho_0 f(1 - f)}, \qquad (33)$$

where the integration is over $-\pi/\Delta_\nu \leq k_\nu \leq \pi/\Delta_\nu$ for $\nu = x, y,$ and z. Furthermore, in the limit of $N \to \infty$,

$$\mathcal{F}(k) \to \frac{N \tanh(k^2 a^2 / 12)}{f(1 - f)}, \qquad (34)$$

and, thus,

$$z_\infty = 1 - \frac{1}{(2\pi)^3 \rho_0} \int \frac{d\mathbf{k}}{\tanh(k^2 a^2 / 12)}. \qquad (35)$$

This expression for z_∞ is, in fact, equivalent to the previous one in Eq. (16), but this is not immediately obvious, given the form of $P(t)$ in Eq. (12). However, if we use the alternative form[32]

$$P(t) = \frac{V_{\mathrm{cell}}}{(2\pi)^3} \int \exp(-x|t|) d\mathbf{k}, \qquad (36)$$

from which Eq. (12) is derived,[32] then the equivalence follows directly from the properties of geometric sums, whereby

$$\sum_{i=-\infty}^{\infty} \exp(-x|i|) = \frac{1}{\tanh(x/2)}. \qquad (37)$$

Although z_∞ can be evaluated numerically using either Eq. (16) or (35), the former is far less computational.

We are now able to remove the UV divergence. The first step is to replace the original Hamiltonian by

$$H_f \equiv \tilde{H}_f - F_{\mathrm{UV}}. \qquad (38)$$

Since F_{UV} is independent of the field, it follows that the resulting free energy is just

$$F = \tilde{F} - F_{\mathrm{UV}}. \qquad (39)$$

The second step is to renormalize the interaction parameter by defining $\chi = z_\infty \chi_b$, which transforms Eq. (31) into the Flory–Huggins expression

$$\frac{F}{n k_B T} = \chi N f(1 - f) \qquad (40)$$

for disordered melts. Hence, the UV divergence is now gone, at least, for small χ_b and large N.

B. Free energy calculations

Although simulations do not generally provide direct access to the free energy, derivatives of the free energy with respect to different parameters, X, of the model can be evaluated using

$$\frac{\partial F}{\partial X} = \left\langle \frac{\partial H_f}{\partial X} \right\rangle, \qquad (41)$$

where the angle brackets denote an ensemble average. Thus, differences in free energy can be evaluated by thermodynamic integration (TI) of the derivatives. Lennon et al.[23] were the first to apply this to FTSs. Here, we use a variation of the method, referred to as continuous TI,[41] in which the integration variable continuously varies by small steps of dX (i.e., $X = X_0 + \ell dX$ for $\ell = 0, 1, 2, \ldots$) during the course of the simulation; our TIs typically involve $\sim 10^6$ steps. Once the simulation is complete, the free energy as a function of X is given by

$$F(X) = F(X_0) + \sum_\ell \frac{\partial H_f}{\partial X} dX. \tag{42}$$

To obtain the free energy at a given point in the phase diagram, Lennon and co-workers simulated the composite Hamiltonian

$$H = \lambda \tilde{H}_f + (1 - \lambda) H_{ec}, \tag{43}$$

where

$$\frac{H_{ec}}{k_B T} = \frac{\rho_0}{\chi_b} \int [W_-(\mathbf{r}) - W_{ec}(\mathbf{r})]^2 d\mathbf{r} \tag{44}$$

is the Hamiltonian for an Einstein crystal of harmonic oscillators. The free energy of the polymeric system relative to that of the Einstein crystal is obtained by integrating

$$\frac{\partial H}{\partial \lambda} = \tilde{H}_f - H_{ec}, \tag{45}$$

over the interval $\lambda = 0$–1. By choosing the prefactor in Eq. (44) to be ρ_0/χ_b, the Einstein crystal has a free energy identical to that of the Hamiltonian in Eq. (17) for a homopolymer melt. Hence, the free energy obtained at $\lambda = 1$ automatically accounts for the UV divergence, without having to subtract F_{UV} from the polymer Hamiltonian. The reference field, $W_{ec}(\mathbf{r})$, controls the morphology. To obtain the free energy of the disordered phase, we set $W_{ec}(\mathbf{r}) = \chi_b N(\frac{1}{2} - f)$. For an ordered phase, we simply add an appropriate modulation that mimics the symmetry of the desired phase.

Once the free energy of the polymeric system is known, the optimum dimensions of the simulation box can be determined by calculating the change in free energy with respect to L_v. This has to be done at constant effective χ, and, therefore, χ_b is continuously updated during the simulation. To account for the changing value of χ_b, we integrate

$$\left.\frac{\partial H_f}{\partial L_v}\right|_\chi = \left.\frac{\partial H_f}{\partial L_v}\right|_{\chi_b} + \frac{\partial H_f}{\partial \chi_b}\frac{\partial \chi_b}{\partial L_v}, \tag{46}$$

where the derivative at constant bare χ_b is given by

$$\frac{L_v}{n k_B T}\left.\frac{\partial H_f}{\partial L_v}\right|_{\chi_b} = -\ln Q - \frac{L_v}{Q}\frac{\partial Q}{\partial L_v} + \frac{\chi_b N}{4} + \frac{N}{V\chi_b}\int W_-^2(\mathbf{r})d\mathbf{r} - \frac{M}{2n}, \tag{47}$$

the next derivative with respect to χ_b is given by

$$\frac{1}{n k_B T N}\frac{\partial H_f}{\partial \chi_b} = \frac{1}{4} - \frac{1}{V}\int \frac{W_-^2(\mathbf{r})}{\chi_b^2}d\mathbf{r} + \frac{M}{2n\chi_b N}, \tag{48}$$

and the final derivative provides the change in χ_b required to maintain a constant χ; the information required to calculate this derivative will be provided shortly. We select L_x as our integration variable, but L_y and L_z are also varied simultaneously to maintain either a fixed volume of the simulation box,[31,41]

$$L_y = \left(\frac{L_{x,0}}{L_x}\right)^{1/2} L_{y,0} \quad \text{and} \quad L_z = \left(\frac{L_{x,0}}{L_x}\right)^{1/2} L_{z,0}, \tag{49}$$

or a fixed shape of the simulation box,

$$L_y = \frac{L_x}{L_{x,0}}L_{y,0} \quad \text{and} \quad L_z = \frac{L_x}{L_{x,0}}L_{z,0}. \tag{50}$$

These volume- and shape-conserving TIs are accomplished via appropriate applications of the chain rule

$$\left.\frac{dH_f}{dL_x}\right|_\chi = \sum_v \left.\frac{\partial H_f}{\partial L_v}\right|_\chi \frac{dL_v}{dL_x}. \tag{51}$$

Note that the volume-conserving TIs can only be applied to phases that have, at least, one direction of translational symmetry. To accommodate this requirement, we will restrict our study to the lamellar and cylindrical phases.

As an alternative to TI, Fredrickson and Delaney[25] recently proposed a direct method of evaluating the free energy based on the identity

$$F = L_v \frac{\partial F}{\partial L_v} - V L_v \frac{\partial}{\partial L_v}\left(\frac{F}{V}\right). \tag{52}$$

Using the previous identity in Eq. (41) and the extensity of the free energy (i.e., $F \propto V$), it follows that

$$\frac{F}{n k_B T} = \frac{L_v}{n k_B T}\left\langle\left.\frac{\partial H_f}{\partial L_v}\right|_\chi\right\rangle. \tag{53}$$

Note that the FTS model used by Fredrickson and Delaney involved finite–range interactions, which allowed them to differentiate at constant χ_b. They also accounted for F_{UV} by scaling the fields rather than subtracting it from the Hamiltonian. Doing so results in the alternative expression

$$\frac{L_v}{n k_B T}\left.\frac{\partial H_f}{\partial L_v}\right|_{\chi_b} = -\ln Q - \frac{L_v}{Q}\frac{\partial Q}{\partial L_v} + \frac{\chi_b N}{4} - \frac{N}{2V}\int W_-(\mathbf{r})\phi_-(\mathbf{r})d\mathbf{r}, \tag{54}$$

but, as required, its ensemble average is identical to that of Eq. (47).

III. RESULTS

Previous studies[30,31] have shown that the UV divergence of the continuous GCM is accurately accounted for by the linear renormalization $\chi = z_\infty\chi_b$. To illustrate that this remains true for discrete chains, Fig. 2 plots the disordered-state structure function

$$\frac{S(k)}{\rho_0 N} = \frac{n}{(\chi_b V)^2}\langle|W_-(\mathbf{k})|^2\rangle - \frac{1}{2\chi_b N} \tag{55}$$

for symmetric diblocks ($N_A = N_B = 45$) from three FTSs, using different grid resolutions, but the same $z_\infty\chi_b N = 10$. The FTSs are performed in cubic simulation boxes of sizes $L_v/R_0 = 4.08$, 4.58, and 5.08 with $40 \times 40 \times 40$ grids, resulting in spacings of $\Delta_v/a = 0.968$, 1.086, and 1.205, respectively. The structure functions for $\bar{N} = 10^4$ and 10^6, corresponding to segment densities of $\rho_0 a^3 = 10.54$ and 105.4, are plotted in the lower and upper panels, respectively. In both cases, the $S(k)$ curves are indistinguishable on the scale of the statistical noise.
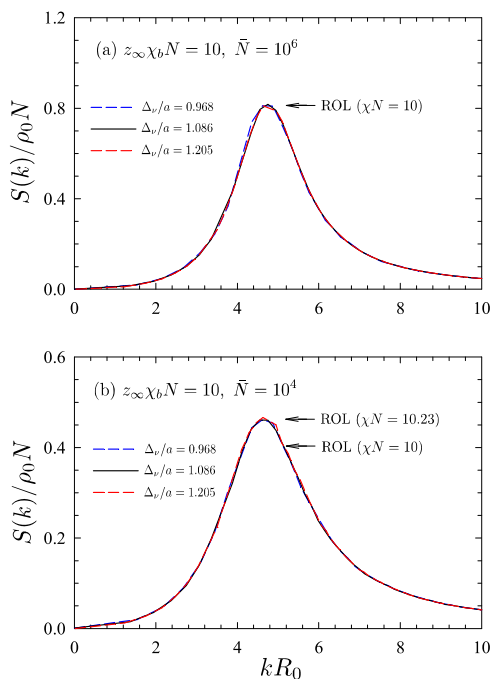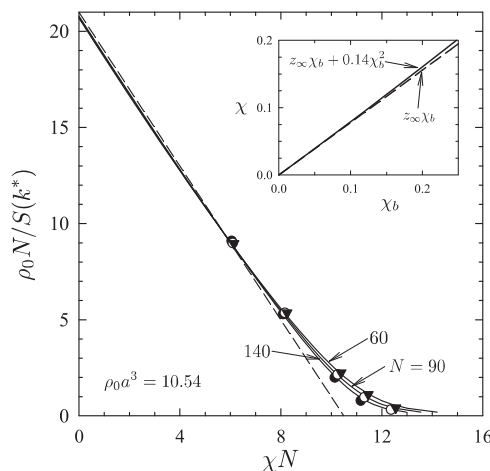
FIG. 2. Structure functions, $S(k)$, for disordered melts of symmetric ($N_A = N_B = 45$) diblock copolymers at (a) $\bar{N} = 10^6$ and (b) $\bar{N} = 10^4$. Results for different grid resolutions, Δ_v, collapse when performed at the same $z_\infty \chi_b N = 10$. Arrows denote peak heights, $S(k^*)$, predicted by ROL theory for different effective χN values.



FIG. 3. Inverse peak height of the structure function, $S^{-1}(k^*)$, plotted in terms of the effective χ for a segment density of $\rho_0 a^3 = 10.54$ and polymerizations of $N = 60$, 90, and 140. Symbols denote FTS results, solid curves are ROL predictions,[35,36] and the dashed line is the RPA prediction.[42] The inset compares the nonlinear χ (solid curve) with its linear approximation (dashed line).

The collapse of the curves implies that two simulation boxes with grid spacings of Δ'_v and Δ_v yield equivalent results, provided that their corresponding bare interaction parameters satisfy

$$\chi'_b \approx \frac{z_\infty}{z'_\infty} \chi_b. \tag{56}$$

However, this does not necessarily imply that the linear approximation of the effective interaction parameter, $\chi \approx z_\infty \chi_b$, is accurate. While the peak height predicted by ROL for $\bar{N} = 10^6$ and $\chi N = 10$ accurately matches the FTS results in Fig. 2(a), the ROL prediction for $\bar{N} = 10^4$ and $\chi N = 10$ underestimates the peak height in Fig. 2(b). According to ROL theory, the observed height corresponds to a somewhat stronger segregation of $\chi N = 10.23$. Hence, the linear χ is slightly inaccurate at the lower segment density, where the fluctuations are more pronounced.

To address this issue, we perform a Morse calibration for $\rho_0 a^3 = 10.54$ and $\Delta_v = 1.086a$. This is done by simulating $S(k)$ for a series of symmetric diblock copolymers of $N = 60$, 90, and 140 at a selection of χ_b values in the disordered region. The peak heights, $S(k^*)$, are then extracted and fit to ROL predictions. Given the large $\bar{N}$ values, we truncate the expansion of χ in Eq. (10) at second order. Figure 3 shows the quality of the fit, and the inset compares the resulting nonlinear $\chi = z_\infty \chi_b + 0.14 \chi_b^2$ to the linear approximation $\chi \approx z_\infty \chi_b$. Note that the nonlinear χ predicts a segregation of $\chi N = 10.23$ for Fig. 2(b), the previous value deduced from the amplitude of $S(k)$.

Although the Morse calibration brings the results into agreement with ROL theory, it potentially needs to be repeated for each distinct grid resolution, which is generally impractical. Fortunately, we have the fact that different grid spacings, Δ'_v and Δ_v, result in identical structure functions, $S(k)$, provided $z'_\infty \chi'_b = z_\infty \chi_b$. It, therefore, follows that the coefficients of a Morse calibration for grid spacings of Δ'_v are given by

$$c'_p = \left(\frac{z'_\infty}{z_\infty} \right)^p c_p \tag{57}$$

in terms of the corresponding coefficients for the grid spacings of $\Delta_v/a = 1.086$. Given this relationship, we can now re-evaluate the fluctuation-corrected ODT from Ref. 3, this time using the nonlinear χ. Figure 4 compares the revised ODT (solid curve) with its original position (dashed curve) shown in Fig. 1. Even though $\bar{N} = 10^4$ is relatively large, the nonlinear term still has a significant effect. In particular, the ODT for symmetric diblocks of $f = 0.5$ shifts from $(\chi N)_{ODT} = 12.71$[43] to 13.12, which is almost identical to the prediction from particle-based simulations, $(\chi N)_{ODT} = 13.11$ (open circle).[9] Although the ODT agrees reasonably well with an analogous prediction for asymmetric diblocks of $f = 0.25$ (open circle),[11] the nonlinear χ does not provide a distinctive improvement over the linear χ; as will be discussed later, this is likely because the particle-based prediction for $f = 0.25$ is less accurate than the one for $f = 0.5$.

Now that we have explained how to translate the Morse calibration between different grid resolutions, the next challenge is to compare free energies at different grid resolutions. Based on previous SCFT calculations[2,39] and FTSs,[3] we will need to evaluate the free energy to an accuracy of about 1 part in 10^4. To begin, we calculate the free energy of symmetric diblocks ($N_A = N_B = 45$) at $z_\infty \chi_b N = 15$ for $\bar{N} = 10^6$ by thermodynamic integration (TI) of Eq. (45). The simulation is performed in a cubic box
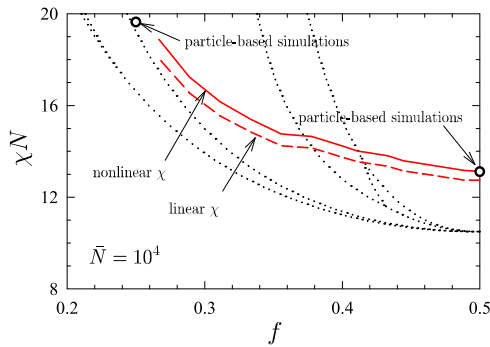
FIG. 4. ODT for $\bar{N} = 10^4$ overlayed on the SCFT phase diagram (dotted curves). Solid and dashed curves are obtained using the nonlinear and linear χ, respectively. Symbols denote predictions from particle-based simulations at $f = 0.5$[9] and $f = 0.25$.[11]

of size $L_v = 4.58R_0$ with a grid of $m_v = 40$, and the Einstein crystal field, $W_{ec}(\mathbf{r})$, is chosen to create three lamellae oriented normal to the x direction. Once the free energy of the polymer system is known, we integrate with respect to L_x using Eq. (51), which varies the lamellar period given by $D = L_x/3$. The solid curve in Fig. 5(a) shows the free energy from volume-conserving TIs (i.e., $L_x L_y L_z$ = constant), while the dashed curve shows the free energy from shape-conserving
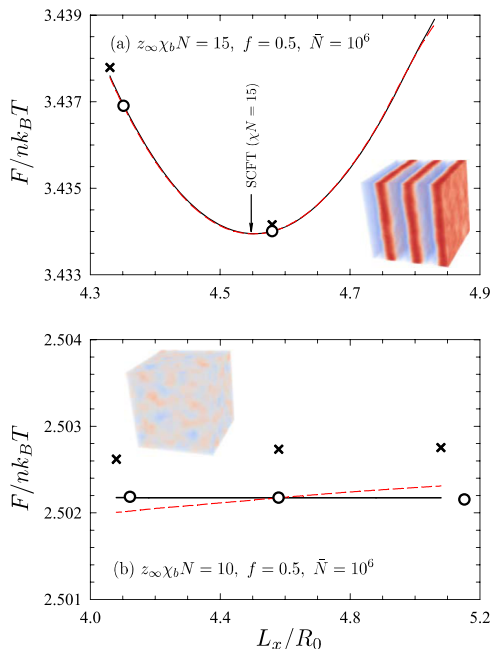
FIG. 5. Free energy, F, of (a) the lamellar phase at $z_\infty \chi_b N = 15$ and (b) the disordered phase at $z_\infty \chi_b N = 10$ for diblock copolymers with $N_A = 45$, $N_B = 45$, and $\bar{N} = 10^6$. Solid and dashed curves are obtained using the volume- and shape-conserving TIs defined by Eqs. (49) and (50), respectively. Circular symbols denote individual TIs from Einstein crystals with identical grid spacing, and crosses denote direct evaluations of F using Eq. (53). Sample configurations are shown with insets.

TIs (i.e., $L_x = L_y = L_z$). The two curves are virtually identical, despite the fact that their grid resolutions are very different, which implies that the UV divergence has been accurately accounted for. We note that there is a small, but noticeable, difference in the free energy at large L_x, but that is not because of the UV difference. It is well known that positive strain causes undulations in the lamellae, so as to reduce the width of the domains.[44] The precise shape of the undulations is sensitive to details, as well as initial conditions, and, consequently, different boxes result in slightly different free energies. Nevertheless, both curves produce consistent free energy minima. Interestingly, the position of the minima coincides with the equilibrium lamellar period, $D_{SCFT} = 1.516R_0$, predicted by SCFT at $\chi N = 15$. Furthermore, the value of the minima closely matches the SCFT prediction of $F_{SCFT} = 3.429nk_BT$.

Figure 5(b) shows analogous results for the disordered phase at $z_\infty \chi_b N = 10$. In this case, the free energy is virtually constant for the volume-conserving TIs (solid line), as should be. However, the free energy from the shape-conserving TIs (dashed line) has a slight positive slope. Although the slope is exceptionally small considering the scale of the vertical axis, the variation in free energy is comparable to the stringent error tolerance required for accurate phase boundary calculations. Nevertheless, the free energy remains reasonably close to the SCFT prediction of $F_{SCFT} = 2.500nk_BT$ for $\chi N = 10$.
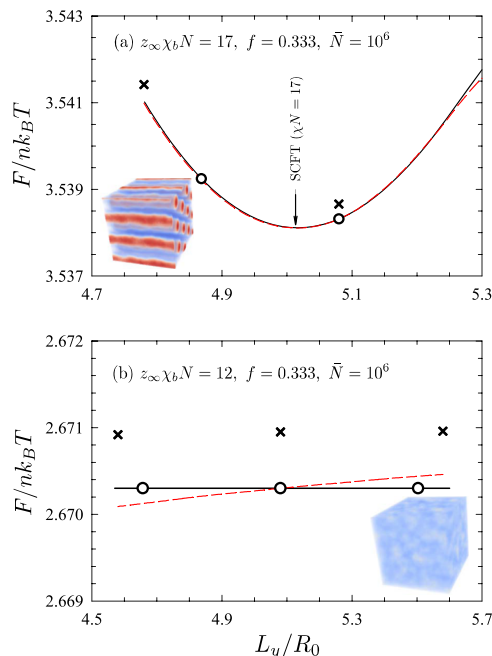
To confirm that the UV divergence has been accurately accounted for, we perform a number of TIs from Einstein crystals (open circles), where the size of the simulation box is varied by adjusting m_v, while maintaining a constant grid spacing of $\Delta_v = 1.086a$. Results for cubic boxes with $m_v = 38$ and 40 at $z_\infty \chi_b N = 15$ agree nicely with the TIs in Fig. 5(a), where the box dimensions were varied by changing the grid spacing. Note that we avoid large boxes of the lamellar phase because of the undulation instability. Analogous results for the disordered phase in cubic boxes of $m_v = 36$, 40, and 45 at $z_\infty \chi_b N = 10$ produce virtually identical free energies, illustrating that finite-size effects are indeed negligible. The results also show that the volume-conserving TIs (solid line) in Fig. 5(b) are accurate, which implies that the small positive slope in the free energy of the shape-conserving TIs (dashed line) is, in fact, an artifact of the UV divergence.

We also test the direct method of calculating the free energy proposed by Fredrickson and Delaney.[25] For the lamellar phase, Eq. (53) is evaluated for the $v = y$ and z directions, in which the morphology is translationally invariant, and the values are then averaged. The resulting free energies (crosses) closely match the TI curves. Note that Eq. (53) cannot be used at large L_v, because the undulations in the lamellae break the translational symmetry in the y and z directions. For the disordered phase, Eq. (53) is evaluated for $v = x$, y, and z, and then averaged. This time, the resulting free energy is somewhat larger than the more accurate TI predictions. Although the difference is tiny in relative terms, the inaccuracy is nevertheless comparable to the error tolerance required for accurate phase boundary calculations.
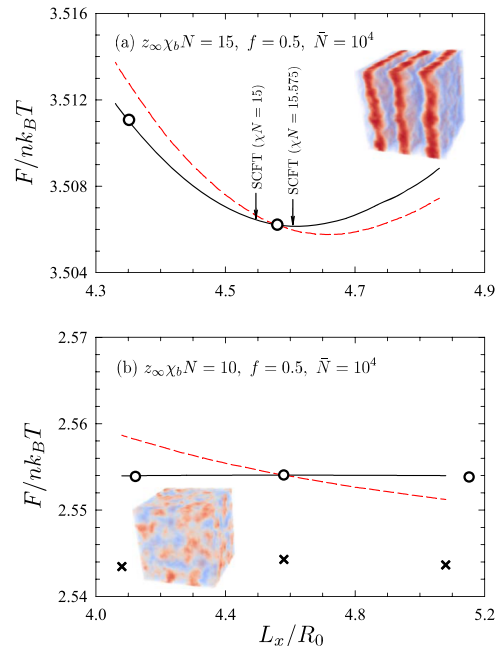
To illustrate the generality of our results, we repeat the previous calculations for lamellar-forming diblocks, but this time for cylinder-forming diblocks ($N_A = 30$ and $N_B = 60$). First, the free energy of an ordered cylinder phase is obtained at $z_\infty \chi_b N = 17$ by performing a TI in an orthorhombic box of size $L_x = L_y = 5.08R_0$ and $L_z = 5.8659R_0$ with a grid of $m_v = 48$ and an Einstein crystal chosen to produce 3×2 unit cells of cylinders with their axes

oriented in the x direction. The spacing between the cylinders is given by $D = L_y/3$. Figure 6(a) then shows the change in free energy as a function of periodicity, obtained using volume-conserving TIs (solid curve) and shape-conserving TIs (dashed curve). Apart from a small discrepancy at large L_y due to the undulation instability, the curves are essentially identical. Just as for the lamellar phase, the curves exhibit free energy minima that accurately match the SCFT prediction of $F_{SCFT} = 3.534 nk_BT$ and $D_{SCFT} = 1.671R_0$ for $\chi N = 17$. Analogous results are shown in Fig. 6(b) for the disordered phase at $z_\infty \chi_b N = 12$. Again, the volume-conserving TIs (solid line) predict a constant free energy, whereas shape-conserving TIs (dashed line) produce a slight positive slope with respect to L_y. TIs performed at a fixed grid resolution of $\Delta_x = \Delta_y = 1.004a$ and $\Delta_z = 1.159a$ (open circles) confirm that the volume-conserving TIs are the accurate ones. In any case, the predicted free energies are close to the SCFT prediction of $F_{SCFT} = 2.667 nk_BT$ for $\chi N = 12$. The direct evaluations of F (crosses) are of similar accuracy as they were for the symmetric diblocks.

We now decrease the invariant polymerization index to an experimentally relevant value of $\bar{N} = 10^4$. Figure 7 shows plots for lamellar-forming diblocks analogous to those in Fig. 5 for the higher $\bar{N}$. The enhanced fluctuations amplify the difference between the volume-conserving TIs (solid curves) and the shape-conserving TIs (dashed curves). TIs at fixed grid resolution (open circles) illustrate that the source of the discrepancy still lies entirely with the
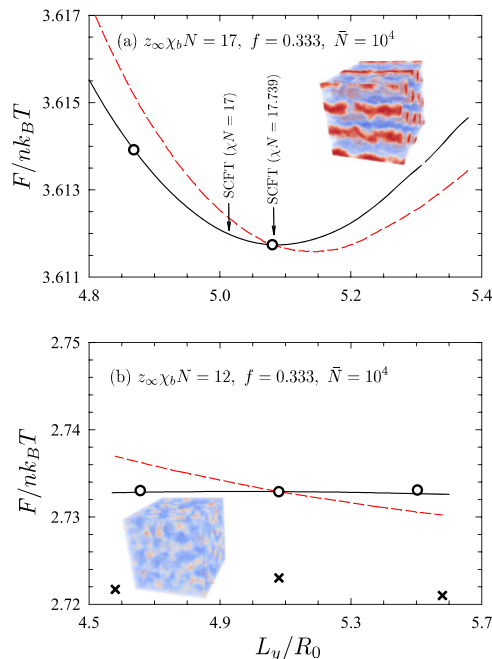

FIG. 7. Analogous plots to those in Fig. 5 for the free energy of the (a) lamellar and (b) disordered phases, but at a reduced invariant polymerization index of $\bar{N} = 10^4$.

shape-conserving TIs. Although the inaccuracy remains relatively modest considering the scales of the vertical axes, it would still affect phase boundary calculations. The direct free energy calculations (crosses) are even more inaccurate, so much so that they are off the scale of Fig. 7(a) for the ordered lamellar phase.

With the increased fluctuations, the SCFT predictions for the lamellar phase at $\chi N = 15$ and the disordered phase at $\chi N = 10$ no longer agree well with the FTS results in Fig. 7. However, the agreement is nicely restored if we evaluate SCFT using the nonlinear χ. For the ordered lamellar phase in Fig. 7(a), the segregation increases to $\chi N = 15.575$, for which SCFT predicts $F_{SCFT} = 3.504 nk_BT$ and $D_{SCFT} = 1.534R_0$. Indeed, the free energy is just slightly above the SCFT prediction, and the position of the minimum almost perfectly matches the arrow corresponding to $3D_{SCFT}$. For the disordered phase in Fig. 7(b), the segregation based on the nonlinear χ is $\chi N = 10.256$, for which SCFT predicts $F_{SCFT} = 2.564 nk_BT$ in reasonable agreement with the FTS.

Figure 8 repeats the calculations in Fig. 6 for cylinder-forming diblocks, but at the reduced invariant polymerization of $\bar{N} = 10^4$. As before, the UV divergence is well accounted for by the volume-conserving TIs (solid curves), as confirmed by the TIs from Einstein crystals, performed with identical grid resolution (open circles). The free energy minimum of the cylinder phase now deviates from the SCFT prediction for $\chi N = 17$ quoted previously, but it agrees well with the prediction of $F_{SCFT} = 3.628 nk_BT$ and $D_{SCFT} = 1.694R_0$ for the $\chi N = 17.739$ obtained using the nonlinear χ. Likewise, the free energy of the disordered phase deviates significantly from the previous SCFT prediction for $\chi N = 12$, but it is close to the $F_{SCFT} = 2.749 nk_BT$ predicted by SCFT for the $\chi N = 12.370$ obtained using the nonlinear χ.

FIG. 6. Free energy, F, of (a) the cylinder phase at $z_\infty \chi_b N = 17$ and (b) the disordered phase at $z_\infty \chi_b N = 12$ for diblock copolymers with $N_A = 30$, $N_B = 60$, and $\bar{N} = 10^6$. Solid and dashed curves are obtained using the volume- and shape-conserving TIs defined by Eqs. (49) and (50), respectively. Circular symbols denote individual TIs from Einstein crystals with identical grid spacings, and crosses denote direct evaluations of F using Eq. (53). Sample configurations are shown with insets.

FIG. 8. Plots analogous to those in Fig. 6 for the free energy of the (a) cylinder and (b) disordered phases, but at a reduced invariant polymerization index of $\bar{N} = 10^4$.
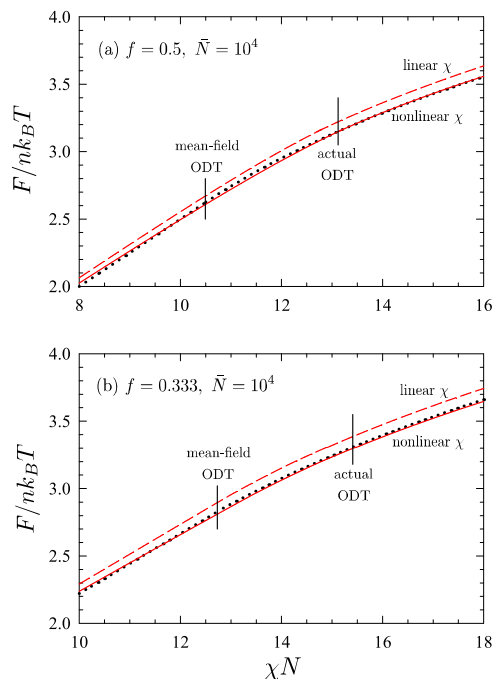
FIG. 9. Free energy for $\bar{N} = 10^4$ compared to that of SCFT for (a) $N_A = 45$ and (b) $N_A = 30$. Solid and dashed curves show the FTS results plotted using the nonlinear and linear χ, respectively, and dotted curves show the SCFT predictions. ODT positions of the FTSs and SCFT are indicated by vertical lines.

The fact that fluctuations shift the position of the ODT implies that the agreement between the free energy of the FTS and SCFT cannot hold over the entire range of χN. Indeed, the free energy of the disordered phase only matches the SCFT prediction, Eq. (40), for χN values below the mean-field ODT in particle-based simulations.[9–11] Between the mean-field and actual ODT, the free energy of the disordered phase crosses over to the SCFT prediction for the ordered phase. To determine what happens in the FTS, we calculate the free energy of the disordered and ordered phases of $f = 0.5$ and 0.333 diblock copolymer melts for $\bar{N} = 10^4$. For the disordered phase, this is done by a TI of the derivative in Eq. (48). For the ordered phases, we generalize the TI to allow the dimensions of the simulation box to track the domain periods predicted by SCFT. The resulting behavior plotted in Fig. 9 is identical to that of particle-based simulations, but only if the FTSs are compared to SCFT using the nonlinear χ.

IV. DISCUSSION

The key facilitating the use of different grid spacings Δ_v' and Δ_v is the fact that a pair of FTSs will produce equivalent, or nearly equivalent, behavior, provided they have a common segment density, ρ_0, and the bare interaction parameters χ_b' and χ_b satisfy Eq. (56). Equivalent behavior implies that the effective χ is the same in both FTSs, but Eq. (56) says nothing about the actual value of χ. It is believed that χ should be independent of molecular details (e.g., N_A and N_B), and, thus, Eq. (10) expresses χ as a simple Taylor series in χ_b. The first coefficient, z_∞, can be evaluated using Eq. (16) or (35), which ensures that the Flory–Huggins expression in Eq. (40) is satisfied in the limit of small χ_b. The remaining coefficients, c_p for $p = 2, 3, \ldots$, are then determined by fitting the FTS to some theoretical prediction of the standard Gaussian-chain model (GCM).

The Morse calibration for c_p uses the ROL prediction of the disordered-state structure function, $S(k)$, because this is thought to be the most accurate prediction available. Although the fit is only performed for symmetric diblocks, the coefficients should be independent of molecular architecture and, thus, should apply to all block copolymers, as is the case for z_∞. Nevertheless, the coefficients will depend on the monomer density and the grid resolution, i.e., $\rho_0 a^3$, Δ_x/a, Δ_y/a, and Δ_z/a. Thus, a new calibration is potentially required for each combination of these four parameters. This is why Beardsley and Matsen[3] evaluated the fluctuation-corrected ODT in Fig. 1 using $\chi \approx z_\infty \chi_b$, since the z_∞ can be calculated analytically. However, given the fact that a pair of FTSs produce the same $S(k)$, provided that they have the same segment density and their bare interactions satisfy Eq. (56), it immediately follows that the coefficients for different grid resolutions are related by Eq. (57). Since the FTSs in Ref. 3 were all performed for $\rho_0 a^3 = 10.54$, the single Morse calibration in Fig. 3 can, in fact, be applied to all the points along the ODT, even though they were calculated with different grid resolutions.

The resulting correction to the ODT in Fig. 4 is relatively modest, but nevertheless significant. As noted previously, it brings the ODT at $f = 0.5$ into excellent agreement with particle-based simulations.[9] It is somewhat difficult to judge the level of agreement with the particle-based simulations at $f = 0.25$,[11] since the FTS results only cover the range $f \geq 0.267$. It appears, though, that the

switch from the linear to nonlinear χ does not produce much of an improvement. This could be partly because the ODT occurs at a higher χ, where the Morse calibrations of the FTSs and the particle-based simulations are undoubtedly less accurate. However, there is good reason to suspect that the particle-based prediction for $f = 0.25$ is relatively inaccurate. First, it relies on a considerable extrapolation from $\bar{N} \lesssim 4000$, whereas the prediction for $f = 0.5$ involves a modest extrapolation from $\bar{N} \lesssim 8000$. Second, the extrapolation for $f = 0.5$ benefits from the Fredrickson–Helfand prediction[18] at large $\bar{N}$.

Our FTSs support the profound conclusion from particle-based simulations[9–11] that the free energy and periodicity of ordered phases are consistent with SCFT. In our case, the free energies from the FTSs agree with SCFT to within ~0.1%, and the preferred domain sizes of the FTSs and SCFT are even too similar to discern. For $\bar{N} = 10^6$, it is sufficient to use the linear χ, but for $\bar{N} = 10^4$, this level of agreement is only achieved when the SCFT is evaluated with the nonlinear χ. We note that the agreement for the cylinder phase is somewhat less than that for the lamellar phase, but this is probably because the nonlinear χ is less accurate at the higher values of χ_b. In any case, the agreement in free energy implies that fluctuations should have a relatively small effect on OOTs. Furthermore, the agreement in domain size is of considerable practical significance; not only are SCFT calculations far less computational, the accurate volume-conserving TIs are not applicable to triply periodic phases (e.g., S, G, and O[70]).

Likewise, we observed similar agreement between FTSs and SCFT for the free energy of the disordered phase. As was the case for the ordered phases, the agreement at $\bar{N} = 10^4$ requires the SCFT prediction, Eq. (40), to be evaluated using the nonlinear χ. However, this agreement does not hold in general, or otherwise it would imply that the ODT is relatively unaffected by fluctuations. As is the case in particle-based simulations,[9–11] the free energy follows the SCFT prediction for the disordered phase up to the mean-field ODT and then switches to the SCFT prediction for the ordered phase up to the actual ODT. Although fluctuations destroy the periodicity of weakly ordered morphologies, they evidently have little effect on the free energy.

The structure functions plotted in Fig. 2 demonstrate that Eq. (56) does an excellent job of mapping between different grid resolutions. It was only when we considered small changes in free energy (i.e., 1 part in 10^4) at the reduced $\bar{N} = 10^4$ that imperfections in the mapping started to appear. Based on our TIs from Einstein crystals with identical grid spacing, we know that the volume-conserving TIs are exceptionally accurate. The problem lies solely with the shape-conserving TIs. Even still, the inaccuracy only represents a slight departure from Eq. (56). For the disordered phase in Fig. 7, the adjustment to z_∞ required to maintain a constant free energy is $\lesssim 0.1\%$.

The reason that the volume-conserving TIs prove to be more accurate than the shape-conserving TIs can be understood by examining the variation in z_∞. In Fig. 7, for instance, z_∞ only varies from 0.7804 to 0.7805 for the volume-conserving TIs (solid line), whereas it ranges from 0.7431 to 0.8065 for the shape-conserving TIs (dashed line). This is because, to an excellent approximation, z_∞ and, thus, the UV divergence are controlled by the volume of the grid cells, $V_{\text{cell}} = \Delta_x \Delta_y \Delta_z$, as opposed to the individual values of Δ_v. Hence, the strength of the UV divergence remains almost constant

for the volume-conserving TIs, as is the case when simulations are performed with identical grid resolutions. The fact that z_∞ is primarily a function of $\rho_0 a^3$ and V_{cell}/a^3 is not particularly surprising, given that it is related to the probability of two monomers from the same chain occupying the same cell of the grid.

The direct estimate of F using Eq. (53) performs well for $\bar{N} = 10^6$, but unfortunately, not so well for $\bar{N} = 10^4$. Apart from statistics, the only potential sources of inaccuracy are finite-size effects and the estimation of $\partial \chi_b / \partial L_v$. Our simulation boxes were sufficiently large that $F \propto V$, and, so, the inaccuracy must originate from Eq. (56) used to evaluate the change in bare χ_b required to maintain a constant effective χ. This is the same source responsible for the inaccuracy of the shape-conserving TIs in Figs. 5–8. Indeed, both inaccuracies can be simultaneously corrected with the same minor adjustment to $\partial \chi_b / \partial L_v$, as must be the case, since Eq. (53) derives from the mathematical identity in Eq. (52).

The effect of V_{cell} on the UV divergence should not seriously impede our ability to evaluate the boundary between two phases. The problem can be avoided, or at least minimized, by selecting the grid spacings, Δ_v' and Δ_v, of the competing phases such that $V_{\text{cell}}' \approx V_{\text{cell}}$ (or rather $z_\infty' \approx z_\infty$). This is far less restrictive than requiring identical grids (i.e., $\Delta_v' = \Delta_v$ for $v = x, y$, and z). For morphologies that have translational symmetry in one of the directions v (e.g., the disordered, L, and C phases), the corresponding Δ_v can be chosen freely, and, therefore, one has the freedom to precisely match its cell volume with that of the competing phase. Potential issues will only arise when comparing two triply periodic–phases (e.g., the G-O[70] phase boundary).

For triply–periodic phases (e.g., S, G, and O[70]), the value of $V_{\text{cell}} = L_x L_y L_z / m_x m_y m_z$ is constrained by the fact that L_v must be commensurate with the equilibrium periodicity of the morphology in the v direction and the fact that m_v must be an integer. Nevertheless, we can accept some difference between V_{cell}' and V_{cell}. Based on Figs. 7(b) and 8(b), a mismatch of $\lesssim 5\%$ should not affect the free energy difference too seriously. In the event that it is not possible to find sufficiently similar values for V_{cell}' and V_{cell}, one could use a metastable morphology, such as the L or C phase, to estimate the effect of the mismatch on the free energy difference. Thus, even boundaries between triply–periodic phases should be manageable.

Delaney and Fredrickson[24] have already calculated complete phase diagrams using FTSs. They avoided the UV divergence by regularizing the Hamiltonian. This was done by smearing the polymer concentrations, which in effect imparts a finite range, a_{int}, to the interactions. As a result, the FTSs converge once the grid spacing becomes small relative to the range of the interactions. However, this comes at a computational cost. To obtain universal results, the range of the interactions needs to be small relative to all other relevant length scales, the shortest of which is undoubtedly the width of the internal A/B interfaces, w_I. Thus, this strategy requires $\Delta_v \ll a_{\text{int}} \ll w_I$, whereas our approach only requires $\Delta_v \ll w_I$. The degree to which these inequalities must be satisfied will depend on the level of accuracy required. Some noted inconsistencies between experiments and the phase diagrams calculated in Ref. 24 may, in fact, be due to not meeting these requirements sufficiently.[3] Choosing the regularization approach would likely require grids of, at least, twice the resolution in each dimension, which would increase the number of grid points, M, by an order of magnitude. On the

other hand, the regularization approach might benefit from the direct method of calculating free energy, where the derivative in Eq. (53) can be performed at constant χ_b, thus avoiding the inaccuracy that we experienced. It remains to be seen which strategy—the renormalization of χ_b or the regularization of H_f— will fare best.

V. SUMMARY

A strategy has been developed for dealing with the UV divergence that occurs in field-theoretic simulations (FTSs) of block copolymer melts. First, the free energy corresponding to the homopolymer limit (i.e., $\chi_b = 0$) is zeroed by removing F_{UV} from the field-based Hamiltonian. Next, an effective interaction parameter, $\chi = z_\infty \chi_b + c_2 \chi_b^2 + c_3 \chi_b^3 + \cdots$, is defined, to account for the reduction in the intermolecular contacts that occurs as the grid resolution becomes finer. The linear coefficient, z_∞, can be evaluated analytically using Eq. (16), but the nonlinear coefficients, c_p, require fits to ROL theory. In principle, the coefficients depend on four parameters: the segment density, $\rho_0 a^3$, and the grid spacings, Δ_ν/a, for $\nu = x$, y, and z. However, to an excellent approximation, they just depend on $\rho_0 a^3$ and $V_{cell}/a^3 = \Delta_x \Delta_y \Delta_z/a^3$.

A key observation is that simulations with different grid spacings, Δ_ν' and Δ_ν, produce equivalent results, and, thus, correspond to equivalent χ, provided that their respective bare interactions, χ_b' and χ_b, satisfy Eq. (56). This leads to the relationship in Eq. (57) relating the coefficients of the nonlinear χ for different grid spacings. Using this, we revised the order–disorder transition (ODT) for $\bar{N} = 10^4$ from the original prediction[3] plotted in Fig. 1 based on the linear χ to a more accurate prediction based on the nonlinear χ derived from the Morse calibration in Fig. 3 for $\Delta_\nu = 1.086a$. Notably, the switch to the nonlinear χ brings the ODT into agreement with particle-based simulations of symmetric ($f = 0.5$) diblock copolymers.[9]

Consistent with particle-based simulations,[9–11] we also find that the free energy and domain size of ordered phases match the predictions of self-consistent field theory (SCFT). However, accurate agreement generally requires the SCFT to be evaluated with the nonlinear χ. The fact that SCFT predicts accurate domain sizes represents a considerable cost saving for FTSs. Furthermore, the fact that the free energy remains similar to SCFT predictions implies that fluctuations will have a relatively small effect on order–order transitions (OOTs), as opposed to the large effect they have on the ODT. Similar agreement between FTSs and SCFT was also observed for the free energy of the disordered phase, but only below the mean-field ODT. Between the mean-field and actual ODT, the free energy of the disordered phase tracks the SCFT prediction for the ordered phase.

The mapping between bare interaction parameters in Eq. (56) works exceptionally well at large $\bar{N} = 10^6$, but slight imperfections appear at $\bar{N} = 10^4$, particularly when the difference between z_∞' and z_∞ is large. Although the discrepancy is relatively small, it could nevertheless prevent accurate phase boundary calculations. This poses a potential issue for OOT calculations, where each ordered phase requires the simulation box to be commensurate with its equilibrium periodicity. Fortunately, however, the inaccuracy becomes negligible when $V_{cell}' \approx V_{cell}$. Provided that one of the competing phases is uniform, singly periodic or doubly periodic, it is generally possible to select grid resolutions such that $V_{cell}' = V_{cell}$. In the event that both phases are triply periodic (e.g., gyroid and Fddd) and it is not

possible to select grids with sufficiently similar cell volumes, a non-triply-periodic metastable phase (e.g., lamellar or cylindrical) could be used to gauge the effect of different cell volumes on the free energy difference. Thus, we now have the means to calculate complete phase diagrams and to map the results onto the standard Gaussian-chain model (GCM) using the Morse calibration of χ.

AUTHOR DECLARATIONS

Conflict of Interest

The authors have no conflicts to disclose.

Author Contributions

M. W. Matsen: Conceptualization (lead); Funding acquisition (lead); Investigation (lead); Methodology (lead); Software (equal); Supervision (lead); Writing – original draft (lead); Writing – review & editing (lead). **T. M. Beardsley**: Investigation (supporting); Software (equal). **J. D. Willis**: Investigation (supporting).

DATA AVAILABILITY

The data that support the findings of this study are available from the corresponding author upon reasonable request.

REFERENCES

[1] F. S. Bates, "Polymer-polymer phase behavior," Science **251**, 898–905 (l991).

[2] M. W. Matsen, "Fast and accurate SCFT calculations for periodic block-copolymer morphologies using the spectral method with Anderson mixing," Eur. Phys. J. E **30**, 361–369 (2009).

[3] T. M. Beardsley and M. W. Matsen, "Fluctuation correction for the order-disorder transition of diblock polymer melts," J. Chem. Phys. **154**, 124902 (2021).

[4] D. A. Hajduk, P. E. Harper, S. M. Gruner, C. C. Honeker, G. Kim, and E. L. Thomas, "The gyroid: A new equilibrium morphology in weakly segregated diblock copolymers," Macromolecules **27**, 4063–4075 (l994).

[5] M. F. Schulz, F. S. Bates, K. Almdal, and K. Mortensen, "Epitaxial relationship for hexagonal-to-cubic phase transition in a block copolymer mixture," Phys. Rev. Lett. **73**, 86–89 (1994).

[6] M. Takenaka, T. Wakada, S. Akasaka, S. Nishitsuji, K. Saijo, H. Shimizu, M. I. Kim, and H. Hasegawa, "Orthorhombic Fddd network in diblock copolymer melts," Macromolecules **40**, 4399–4402 (2007).

[7] Y.-C. Wang, K. Matsuda, M. I. Kim, A. Miyoshi, S. Akasaka, S. Nishitsuji, K. Saijo, H. Hasegawa, K. Ito, T. Hikima, and M. Takenaka, "Fddd phase boundary of polystyrene-block-polyisoprene diblock copolymer melts in the polystyrene-rich region," Macromolecules **48**, 2211–2216 (2015).

[8] J. Glaser, J. Qin, P. Medapuram, M. Müller, and D. C. Morse, "Test of a scaling hypothesis for the structure factor of disordered diblock copolymer melts," Soft Matter **8**, 11310–11317 (2012).

[9] J. Glaser, P. Medapuram, T. M. Beardsley, M. W. Matsen, and D. C. Morse, "Universality of block copolymer melts," Phys. Rev. Lett. **113**, 068302 (2014).

[10]P. Medapuram, J. Glaser, and D. C. Morse, "Universal phenomenology of symmetric diblock copolymers near the order-disorder transition," Macromolecules **48**, 819–839 (2015).

[11]T. Ghasimakbari and D. C. Morse, "Order-disorder transitions and free energies in asymmetric diblock copolymers," Macromolecules **53**, 7399–7409 (2020).

[12]M. W. Matsen, "The standard Gaussian model for block copolymer melts," J. Phys.: Condens. Matter **14**, R21–R47 (2002).

[13]G. H. Fredrickson, *The Equilibrium Theory of Inhomogeneous Polymers* (Oxford University Press, New York, 2006).

[14]M. W. Matsen, in *Soft Matter: Polymer Melts and Mixtures*, edited by G. Gompper and M. Schick (Wiley VCH, Weinheim, Germany, 2006).

[15]M. W. Matsen, "Field-theoretic approach for block polymer melts: SCFT and FTS," J. Chem. Phys. **152**, 110901 (2020).

[16]E. Helfand, "Theory of inhomogeneous polymers: Fundaments of the Gaussian random-walk model," J. Chem. Phys. **62**, 999–1005 (1975).

[17]J. Qin and D. C. Morse, "Fluctuations in symmetric diblock copolymers: Testing theories old and new," Phys. Rev. Lett. **108**, 238301 (2012).

[18]G. H. Fredrickson and E. Helfand, "Fluctuation effects in the theory of microphase separation in block copolymers," J. Chem. Phys. **87**, 697–705 (1987).

[19]F. S. Bates, M. F. Schulz, A. K. Khandpur, S. Förster, and J. H. Rosedale, "Fluctuations, conformational asymmetry and block copolymer phase behaviour," Faraday Discuss. **98**, 7–18 (1994).

[20]J. D. Willis, T. M. Beardsley, and M. W. Matsen, "A simple and accurate method to determine the Flory-Huggins χ parameter," Macromolecules **53**, 9973–9982 (2020).

[21]G. H. Fredrickson, V. Ganesan, and F. Drolet, "Field-theoretic computer simulation methods for polymers and complex fluids," Macromolecules **35**, 16–39 (2002).

[22]V. Ganesan and G. H. Fredrickson, "Field-theoretic polymer simulations," Europhys. Lett. **55**, 814–820 (2001).

[23]E. M. Lennon, K. Katsov, and G. H. Fredrickson, "Free energy evaluation in field-theoretic polymer simulations," Phys. Rev. Lett. **101**, 138302 (2008).

[24]K. T. Delaney and G. H. Fredrickson, "Recent developments in fully fluctuating field-theoretic simulations of polymer melts and solutions," J. Phys. Chem. B **120**, 7615–7634 (2016).

[25]G. H. Fredrickson and K. T. Delaney, "Direct free energy evaluation of classical and quantum many-body systems via field-theoretic simulation," Proc. Natl. Acad. Sci. U. S. A. **119**, e2201804119 (2022).

[26]E. Reister, M. Müller, and K. Binder, "Spinodal decomposition in a binary polymer mixture: Dynamic self-consistent-field theory and Monte Carlo simulations," Phys. Rev. E **64**, 041804 (2001).

[27]D. Düchs, V. Ganesan, G. H. Fredrickson, and F. Schmid, "Fluctuation effects in ternary AB + A + B polymeric emulsions," Macromolecules **36**, 9237–9248 (2003).

[28]M. W. Matsen and T. M. Beardsley, "Field-theoretic simulations for block copolymer melts using the partial saddle-point approximation," Polymers **13**, 2437 (2021).

[29]M. Olvera de la Cruz, S. F. Edwards, and I. C. Sanchez, "Concentration fluctuations in polymer blend thermodynamics," J. Chem. Phys. **89**, 1704–1708 (1988).

[30]P. Stasiak and M. W. Matsen, "Monte Carlo field-theoretic simulations for melts of symmetric diblock copolymer," Macromolecules **46**, 8037–8045 (2013).

[31]B. Vorselaars, P. Stasiak, and M. W. Matsen, "Field-theoretic simulation of block copolymers at experimentally relevant molecular weights," Macromolecules **48**, 9071–9080 (2015).

[32]T. M. Beardsley and M. W. Matsen, "Calibration of the Flory-Huggins interaction parameter in field-theoretic simulations," J. Chem. Phys. **150**, 174902 (2019).

[33]J. Qin and D. C. Morse, "Renormalized one-loop theory of correlations in polymer blends," J. Chem. Phys. **130**, 224902 (2009).

[34]J. Glaser, P. Medapuram, and D. C. Morse, "Collective and single-chain correlations in disordered melts of symmetric diblock copolymers: Quantitative comparison of simulations and theory," Macromolecules **47**, 851–869 (2014).

[35]P. Grzywacz, J. Qin, and D. C. Morse, "Renormalization of the one-loop theory of fluctuations in polymer blends and diblock copolymer melts," Phys. Rev E **76**, 061802 (2007).

[36]J. Qin, P. Grzywacz, and D. C. Morse, "Renormalized one-loop theory of correlations in disordered diblock copolymers," J. Chem. Phys. **135**, 084902 (2011).

[37]T. M. Beardsley, R. K. W. Spencer, and M. W. Matsen, "Computationally efficient field-theoretic simulations for block copolymer melts," Macromolecules **52**, 8840–8848 (2019).

[38]M. W. Matsen, "Self-consistent field theory for melts of low-molecular-weight diblock copolymer," Macromolecules **45**, 8502–8509 (2012).

[39]P. Stasiak and M. W. Matsen, "Efficiency of pseudo-spectral algorithms with Anderson mixing for the SCFT of periodic block-copolymer phases," Eur. Phys. J. E **34**, 110 (2011).

[40]D. J. Audus, K. T. Delaney, H. D. Ceniceros, and G. H. Fredrickson, "Comparison of pseudospectral algorithms for field-theoretic simulations of polymers," Macromolecules **46**, 8383–8391 (2013).

[41]R. K. W. Spencer, B. Vorselaars, and M. W. Matsen, "Continuous thermodynamic integration in field-theoretic simulations of structured polymers," Macromol. Theory Simul. **26**, 1700036 (2017).

[42]L. Leibler, "Theory of microphase separation in block copolymers," Macromolecules **13**, 1602–1617 (1980).

[43]T. M. Beardsley and M. W. Matsen, "Well-tempered metadynamics applied to field-theoretic simulations of diblock copolymer melts," J. Chem. Phys. **157**, 114902 (2021).

[44]A. Makke, M. Perez, O. Lame, and J.-L. Barrat, "Nanoscale buckling deformation in layered copolymer materials," Proc. Natl. Acad. Sci. U. S. A. **109**, 680–685 (2011).